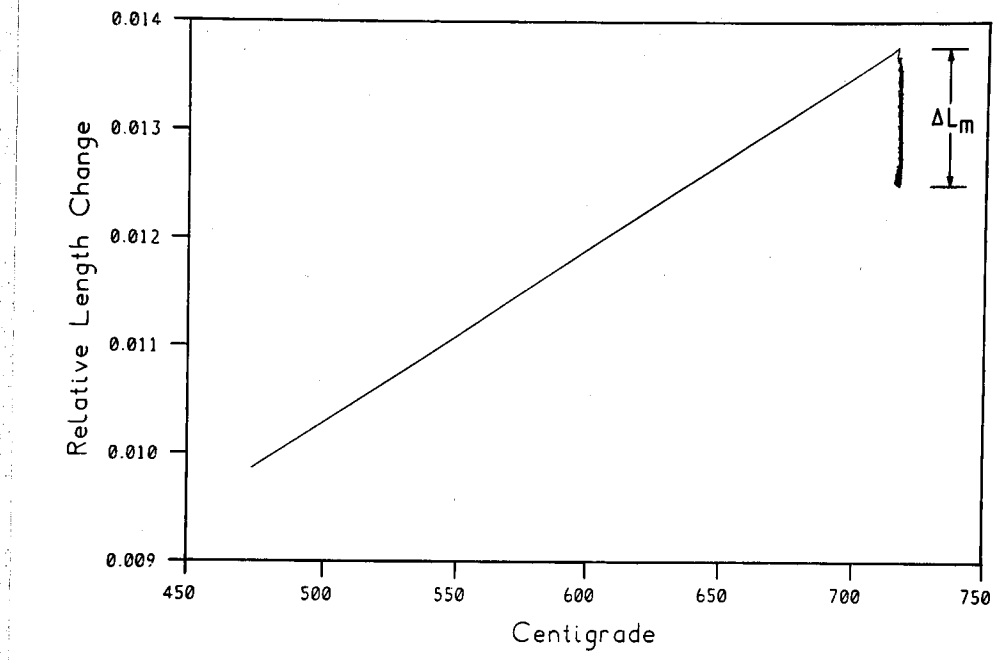

Figure IV.4(a) - The relative length change versus temperature curve for isothermal reaustenitisation at 715°C (from starting microstructure $\alpha_a+\gamma$). The maximum relative length change (ΔL_m) can be directly measured.

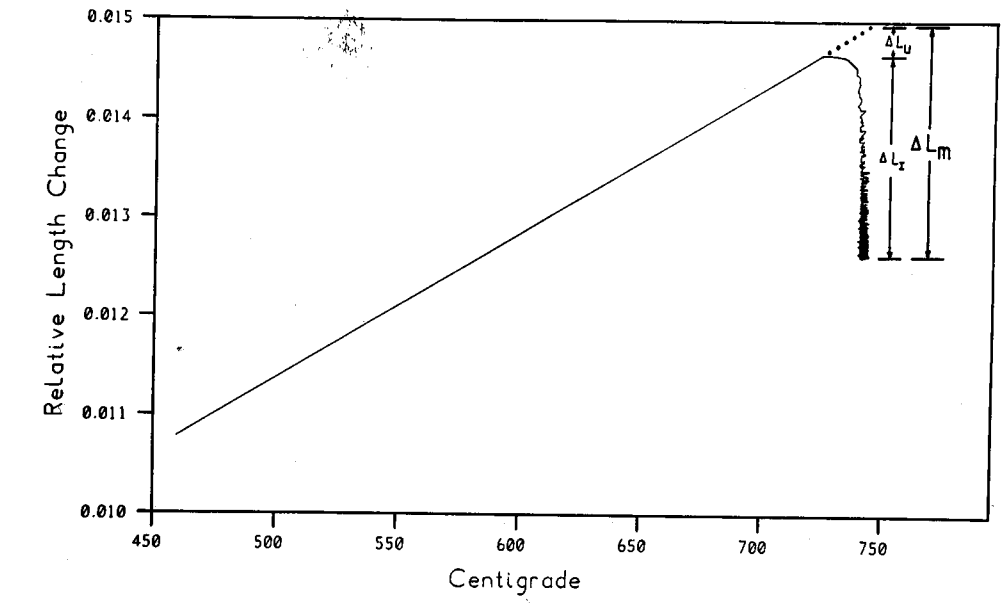

Figure IV.4(b) - The relative length change versus temperature curve for isothermal reaustenitisation at 735°C (from starting microstructure $\alpha_a+\gamma$). ΔL_u is the relative length change due to transformation during the up-quench. ΔL_I is the relative length change during isothermal transformation. Therefore the maximum relative length change $\Delta L_m = \Delta L_u + \Delta L_I$.

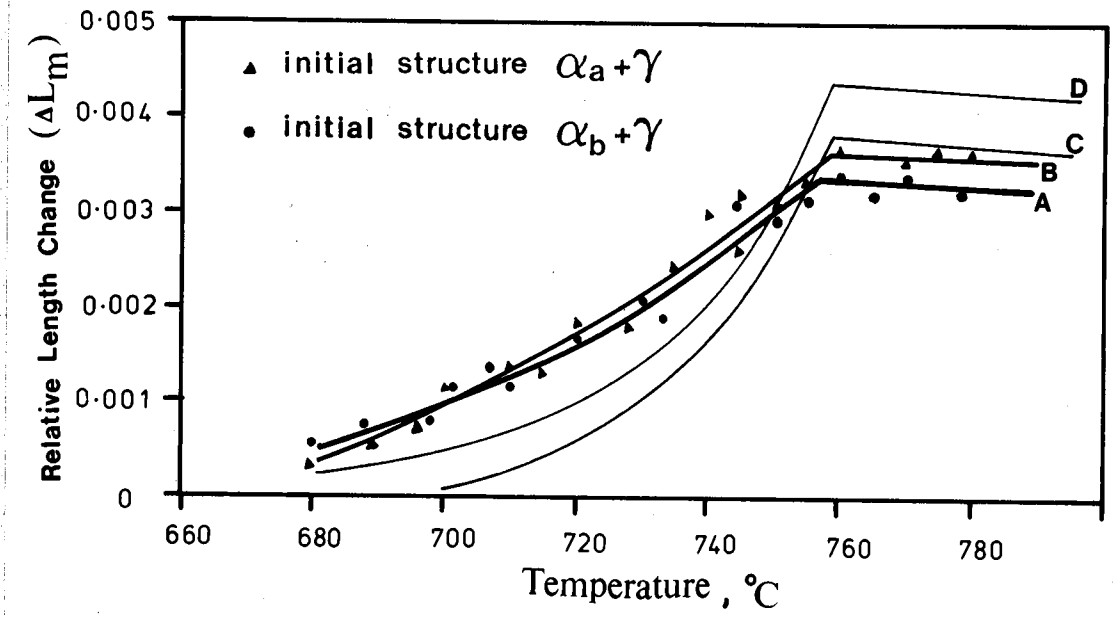

Figure IV.5 - Plot of ΔL_m versus isothermal reaustenitisation temperature. The curve A and B show the experimental data for starting microstructures $\alpha_b+\gamma$ and $\alpha_a+\gamma$, respectively. The calculated curves C and D assume that the α_b (or α_a) reaction stops at the T_o curve or T'_o curve of the phase diagram, respectively.

Figure IV.6(a) - Reaustenitisation at 680°C for 2 hours from starting microstructure $\alpha_b+\gamma$.

Figure IV.6(b) - Reaustenitisation at 700°C for 2 hours from starting microstructure $\alpha_b+\gamma$.

Figure IV.6(c) - Reaustenitisation at 720°C for 2 hours from starting microstructure $\alpha_b+\gamma$.

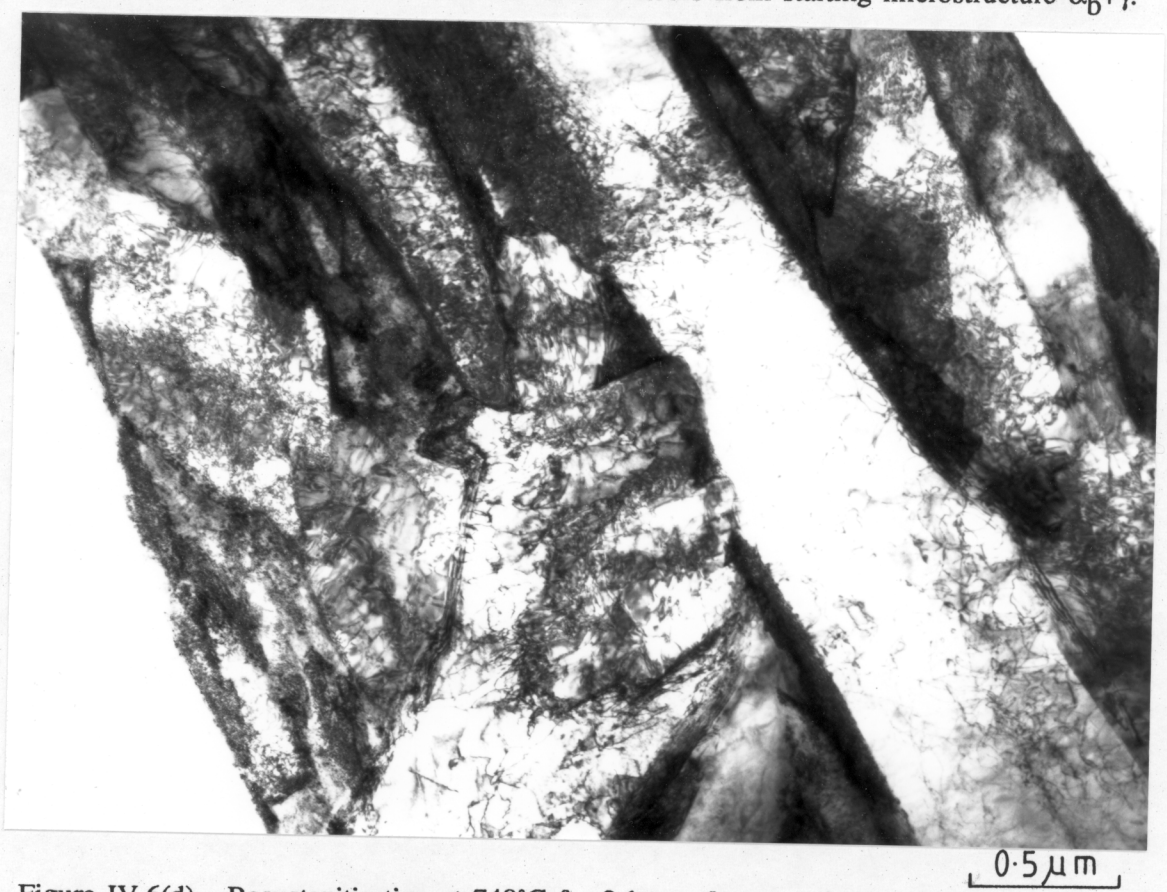

Figure IV.6(d) - Reaustenitisation at 740°C for 2 hours from starting microstructure $\alpha_b+\gamma$.

Figure IV.6(e) - Reaustenitisation at 750°C for 2 hours from starting microstructure $\alpha_b+\gamma$.

Figure IV.6(f) - Reaustenitisation at 760°C for 2 hours from starting microstructure $\alpha_b+\gamma$.

Figure IV.7(a) - Reaustenitisation at 680°C for 10 minutes from starting microstructure $\alpha_a+\gamma$.

Figure IV.7(b) - Reaustenitisation at 700°C for 10 minutes from starting microstructure $\alpha_a+\gamma$.

Figure IV.7(c) - Reaustenitisation at 720°C for 2 hours from starting microstructure $\alpha_a+\gamma$.

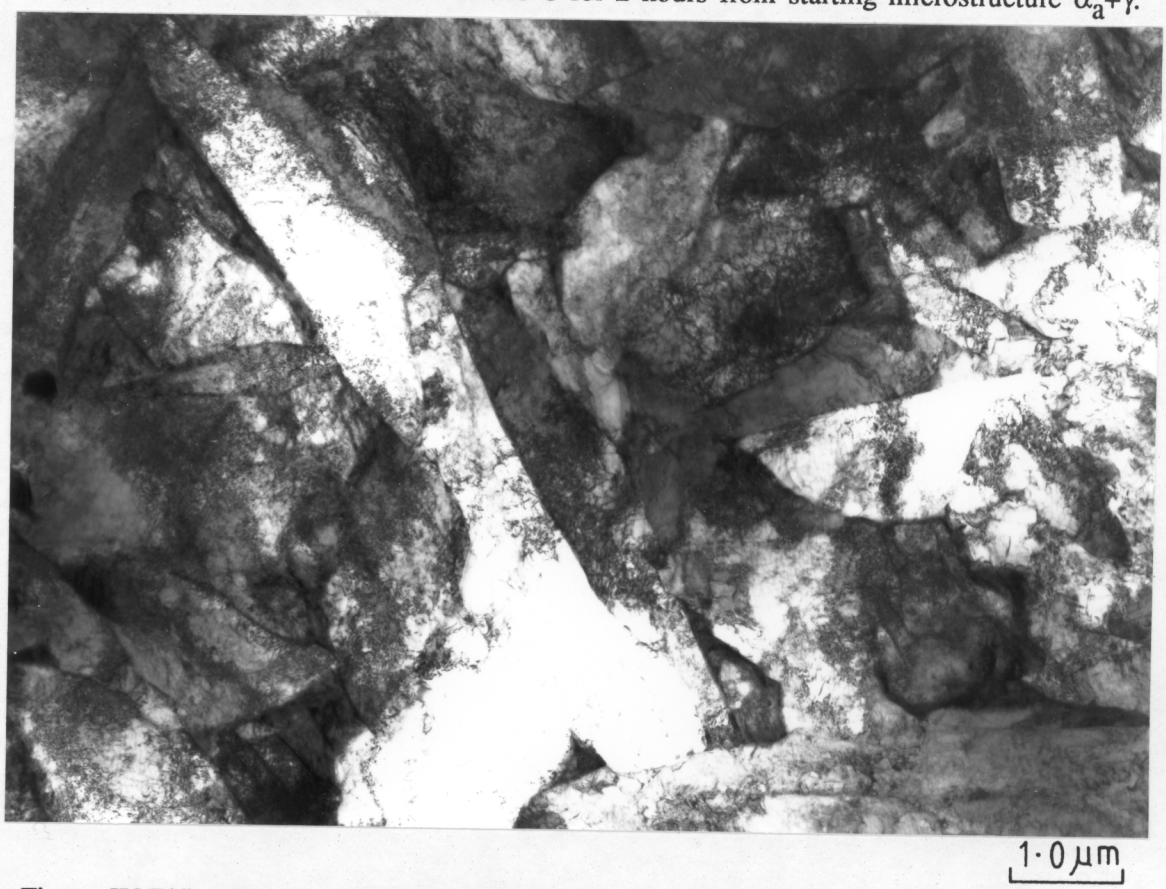

Figure IV.7(d) - Reaustenitisation at 740°C for 2 hours from starting microstructure $\alpha_a+\gamma$.

Figure IV.7(e) - Reaustenitisation at 760°C for 2 hours from starting microstructure $\alpha_a+\gamma$.

Figure IV.7(f) - Reaustenitisation at 770°C for 2 hours from starting microstructure $\alpha_a+\gamma$.

Table IV.1 - Microanalytical Data (wt%, error ≈ ± 0.20) for the γ and α during reaustenitisation from starting microstructure $\alpha_b+\gamma$.

Reaustenitisation Temperature(°C)	Time(min)	Mn γ	Mn α	Ni γ	Ni α
680	10	2.50	1.73	2.98	2.45
730	10	2.29	1.36	2.80	2.24
760	0.67	1.75	1.72	2.66	2.62
710	120	2.39	1.09	3.26	1.96
735	120	2.17	1.23	3.00	1.94
760	120	1.83	1.76	2.57	2.65

Table IV.2 - Microanalytical Data (wt%, err ≈ ± 0.15) for the γ and α during reaustenitisation from starting microstructure $\alpha_a+\gamma$.

Reaustenitisation Temperature(°C)	Time(min)	Mn γ	Mn α	Ni γ	Ni α
680	10	2.83	1.79	2.86	2.31
735	10	2.46	1.64	2.69	2.12
760	2	1.93	1.97	2.58	2.50
715	120	2.73	1.39	2.87	1.89
735	120	2.82	1.42	3.05	1.85
760	120	1.97	1.96	2.44	2.44

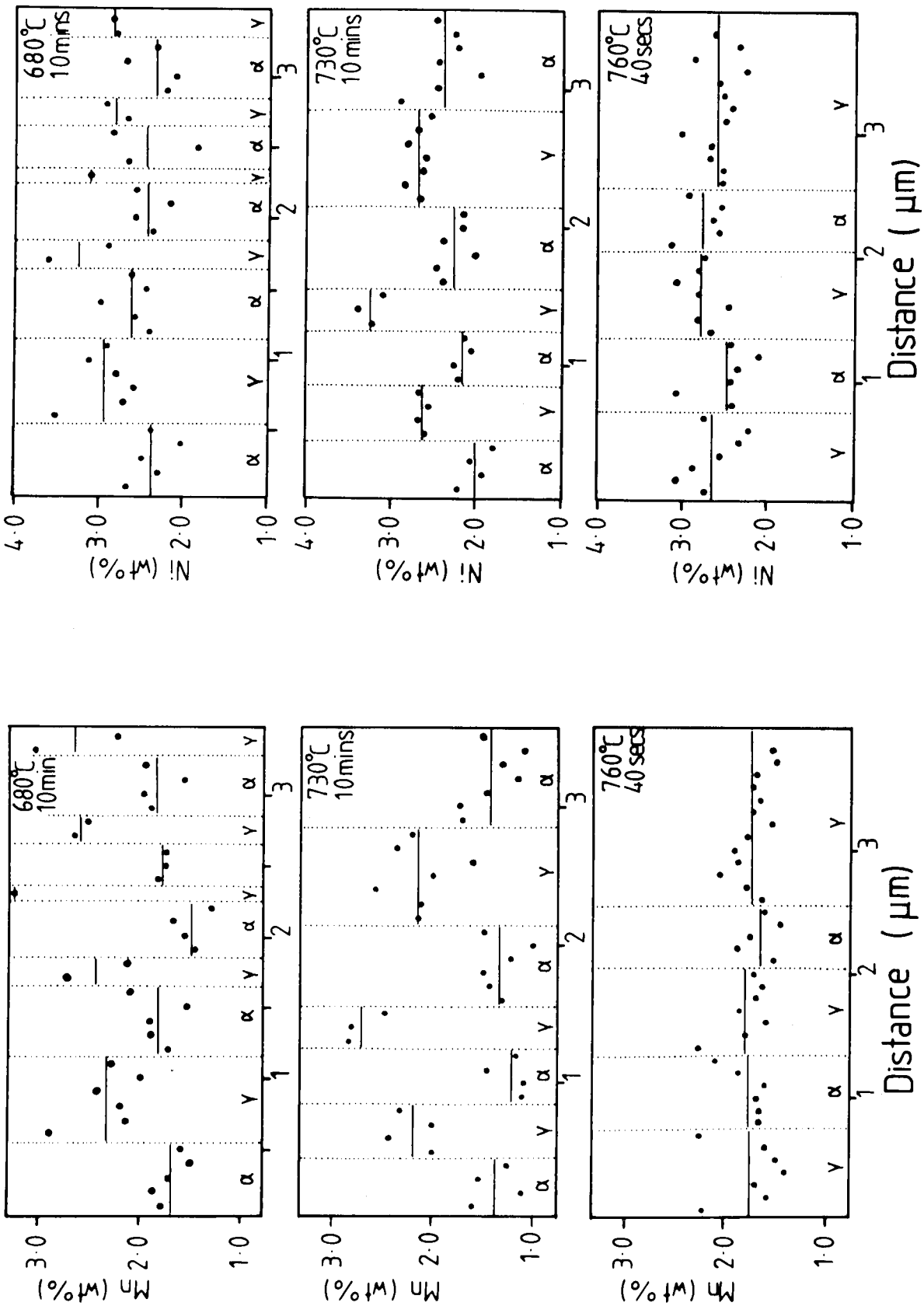

Figure IV.8(a) - Microanalytical data obtained using energy dispersive X-ray analysis on Philips EM400T for specimens reaustenitised from starting microstructure $\alpha_b+\gamma$.

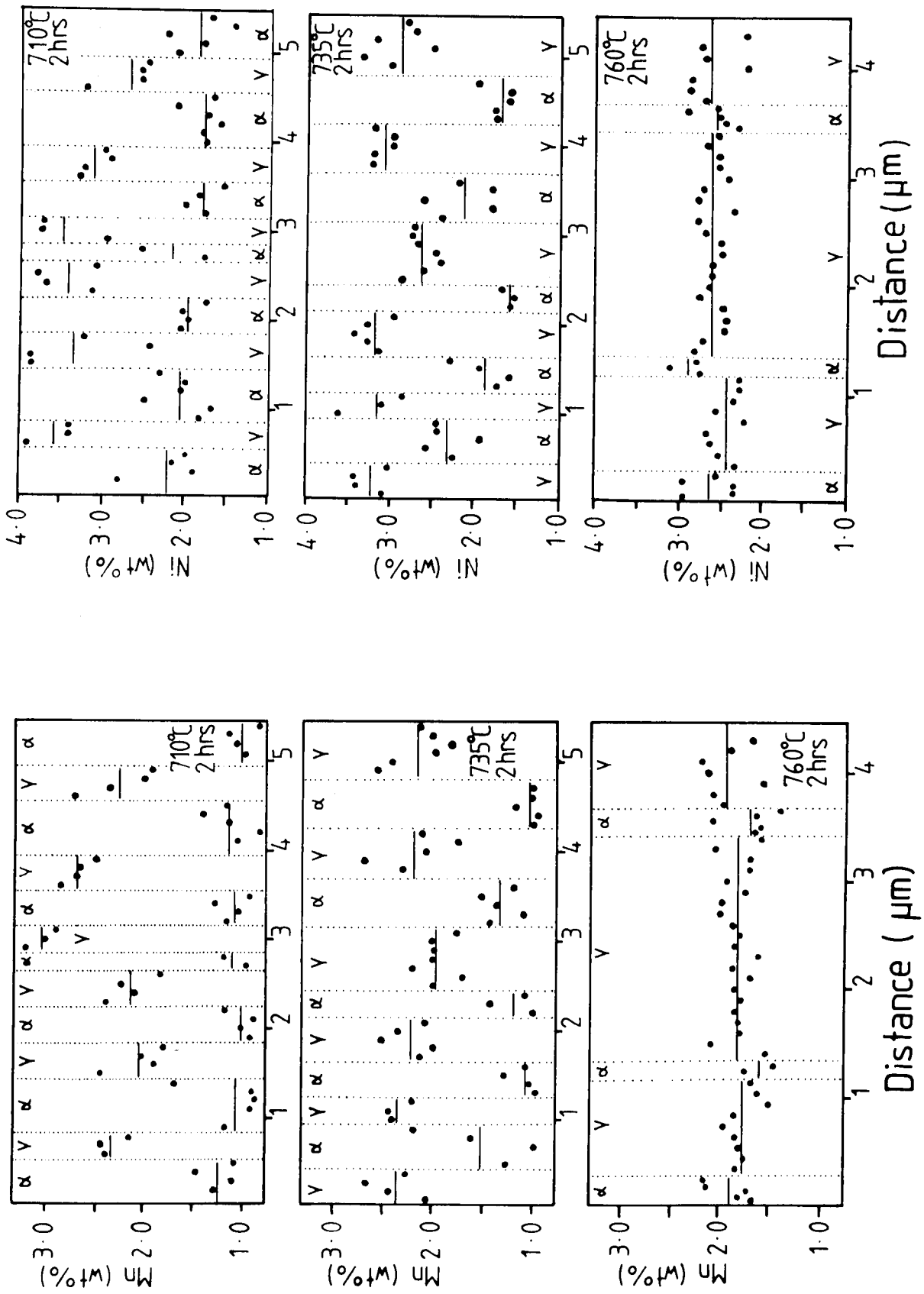

Figure IV.8(b) - Microanalytical data obtained using energy dispersive X-ray analysis on Philips EM400T for specimens reaustenitised from starting microstructure $\alpha_b+\gamma$.

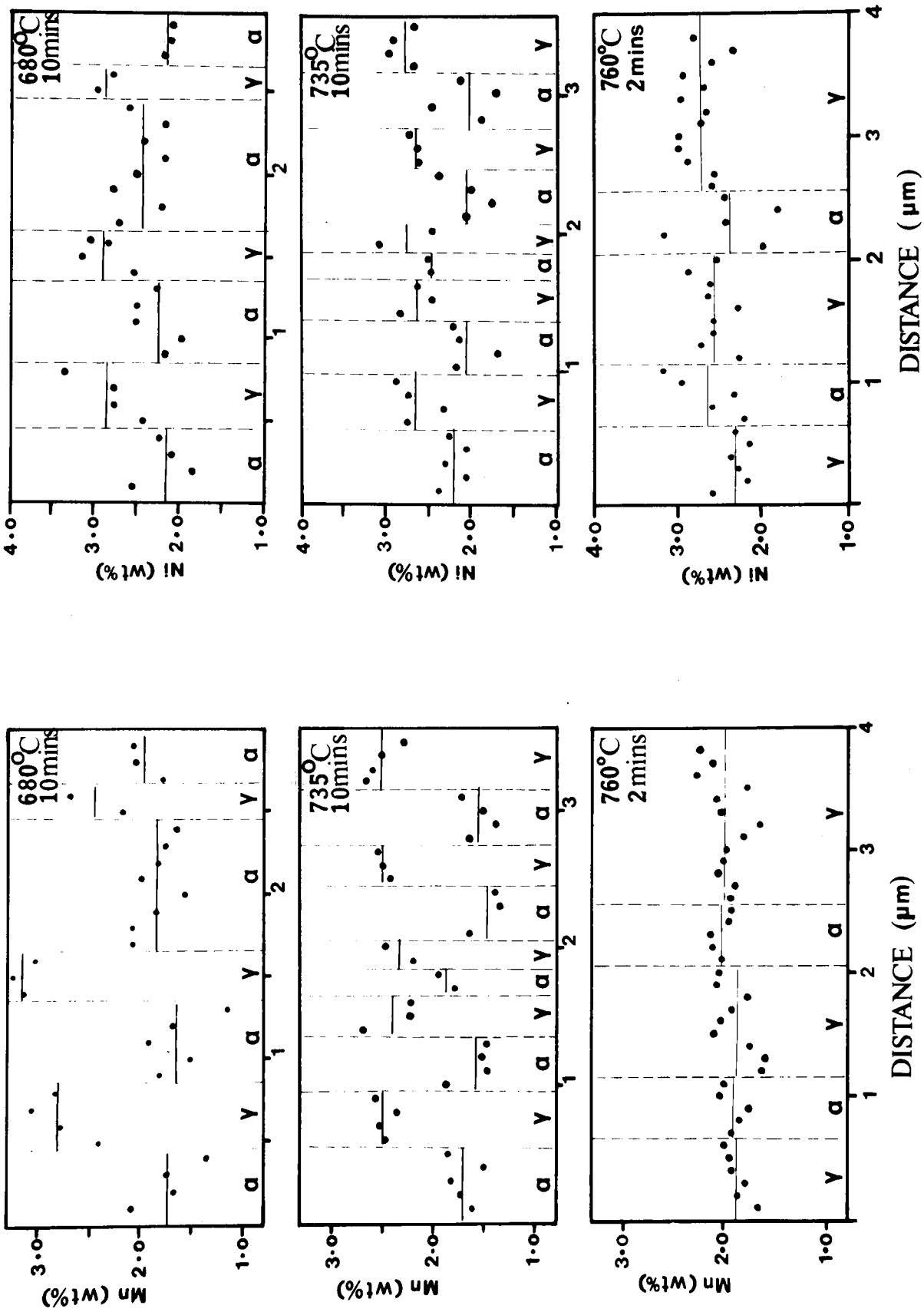

Figure IV.9(a) - Microanalytical data obtained using dispersive X-ray on Philips EM400T for specimens reaustenitised from starting microstructure $\alpha_a+\gamma$.

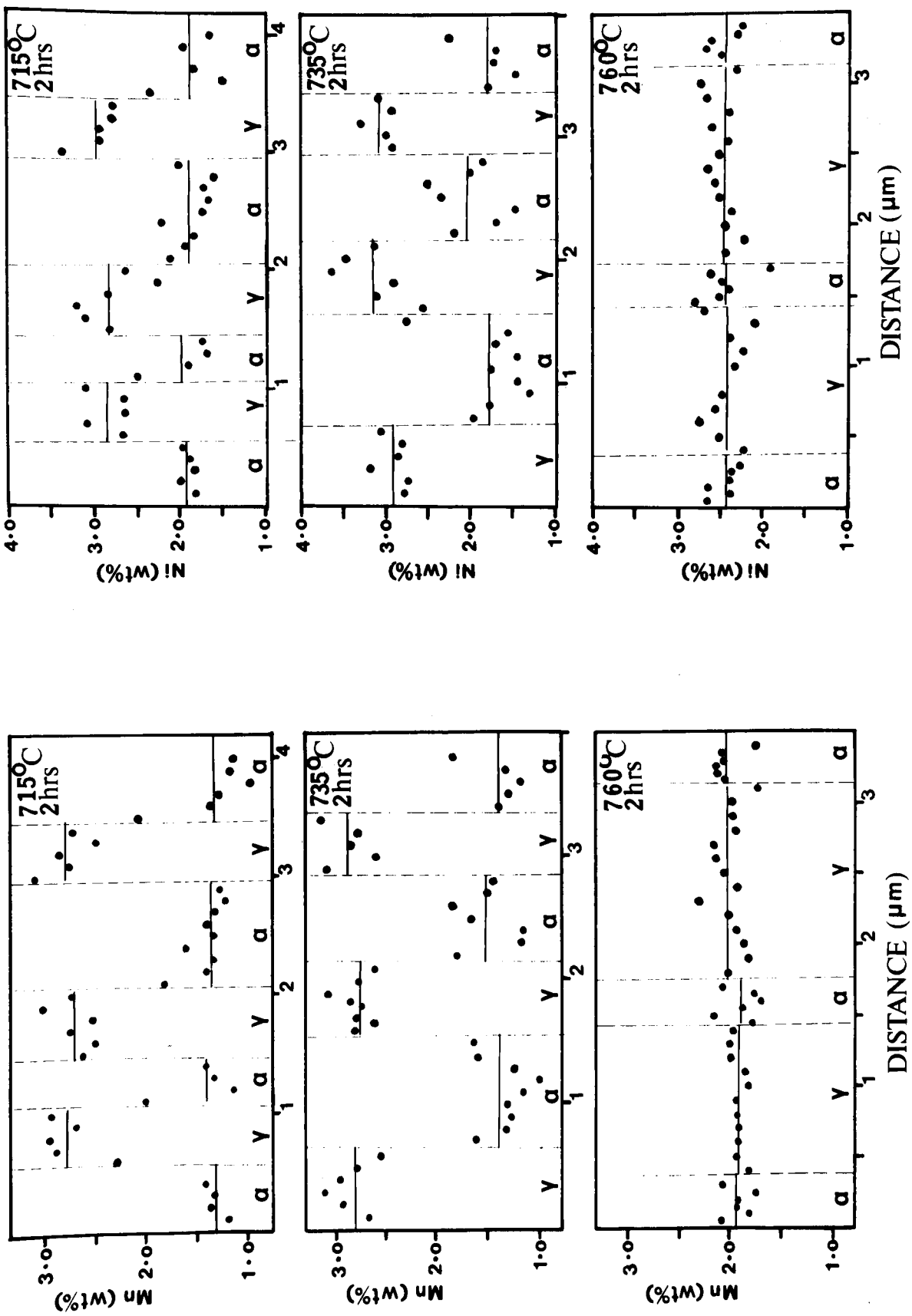

Figure IV.9(b) - Microanalytical data obtained using energy dispersive X-ray anaylsis on Philips EM400T for specimens reaustenitised from starting microstructure $\alpha_a+\gamma$.

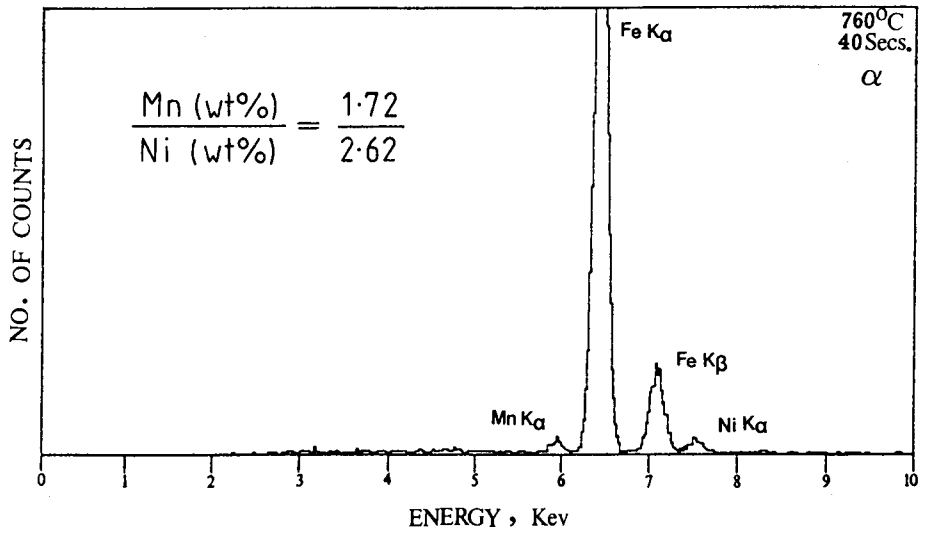

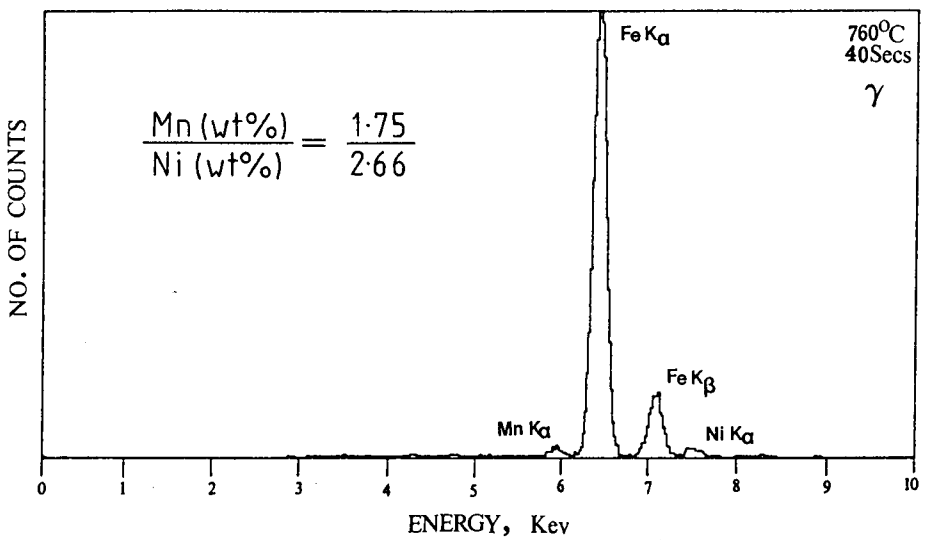

Figure IV.10(a) - Showing the energy dispersive X-ray spectra for the specimen (starting microstructure $\alpha_b+\gamma$) reaustenitised at 760°C for 40 secs. in the α and γ phase respectively.

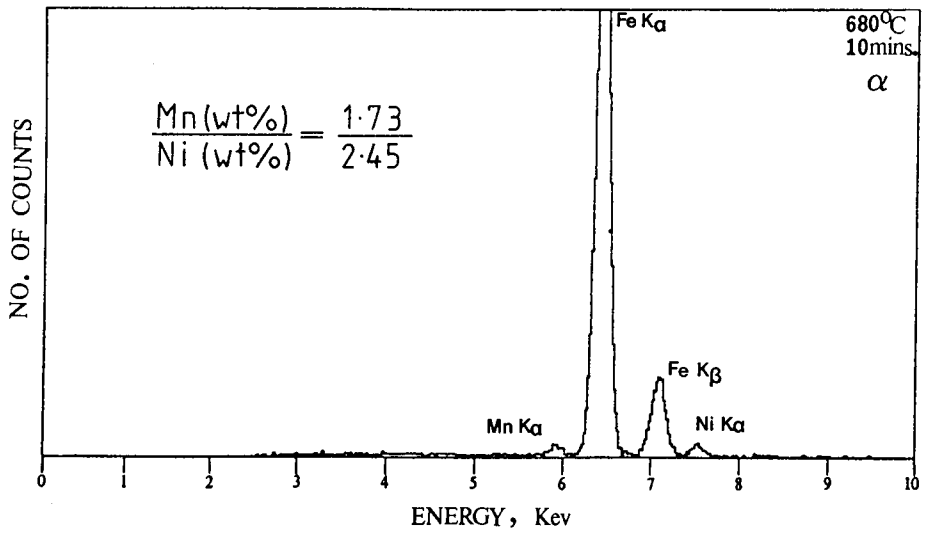

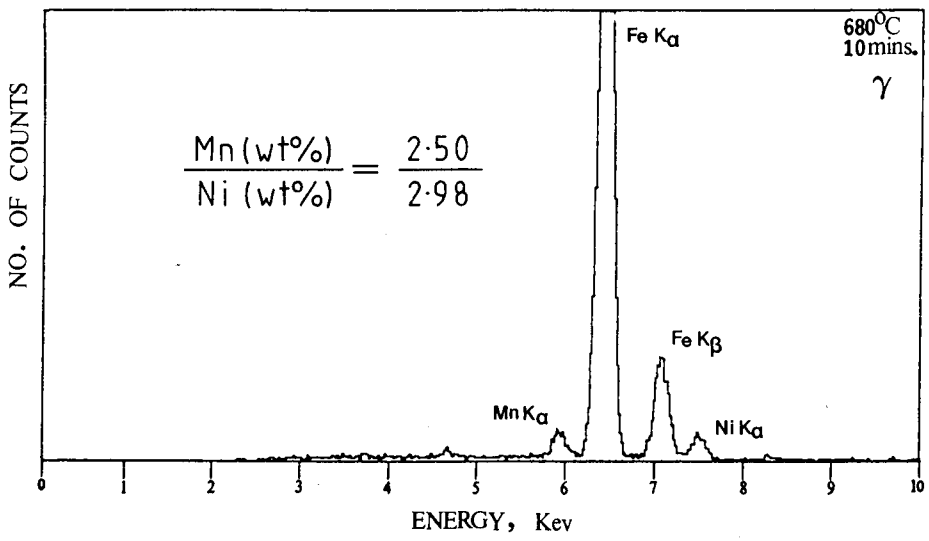

Figure IV.10(b) - Showing the energy dispersive X-ray spectra for the specimen (starting microstructure $\alpha_b+\gamma$) reaustenitised at 680°C for 10 mins. in the α and γ phase respectively.

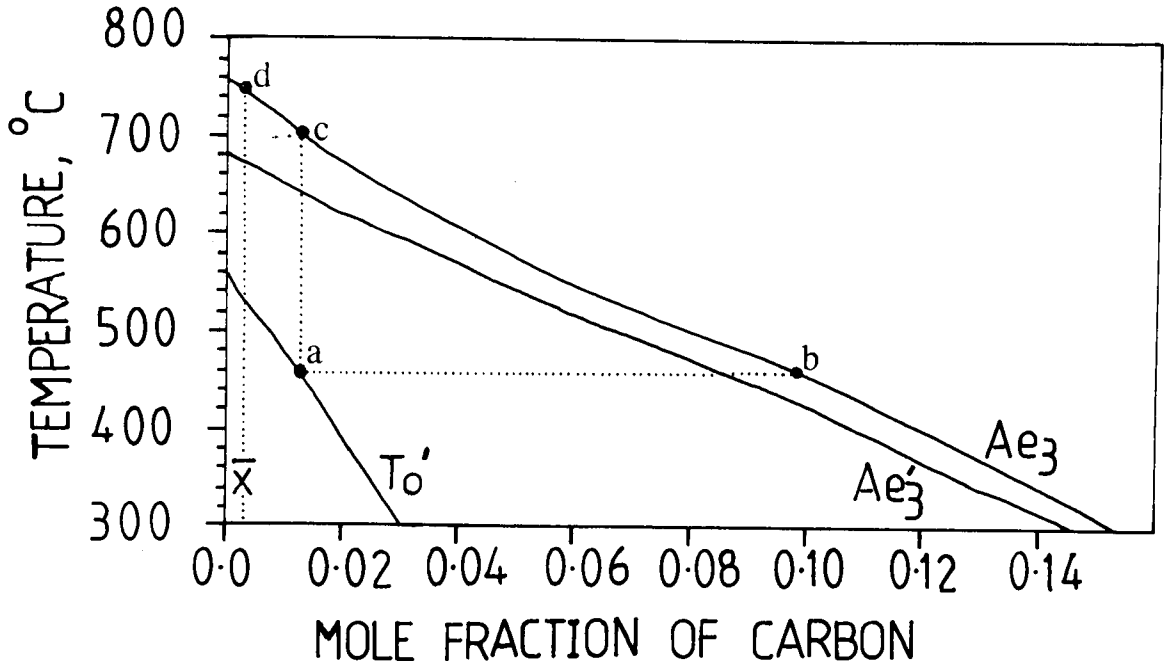

Figure IV.11 - Phase diagram showing the Ae3, Ae3', T_0 and T'_0 curves for a Fe-0.27Si-1.84Mn-2.48Ni-0.20Mo wt% alloy. The Ae3', T_0 and T'_0 curves are calculated as in Ref. 89,100 and the Ae3 is calculated as in Ref. 179

Intercept of T_0 = B_{T_0}

-8542 °C/mole fraction carbon $558 - 3$

Slope of Ae3 line = -3625 °C/mole fraction for T range 758-

Intercept of Ae3 = B_A

$\therefore \quad x_{T_0} = B_{T_0} - 8542\,(T)$

$x_{Ae3} = B_A - 3625\,(T)$

$\therefore$ Austenitisation begins at an temp T_γ, for an alloy isothermally transformed at T_a when

$$x_{Ae3} = B_{T_0} - 8542(T_A) = B_A - 3625(T_\gamma)$$

$$\therefore \quad T_\gamma = \frac{(B_{T_0} - B_A) - 8542\,T_a}{-3625}$$

$$\therefore \quad \frac{\partial T_\gamma}{\partial T_a} = \frac{8542}{3625}$$

Chapter Five

REAUSTENITISATION IN STEEL WELD DEPOSITS - PART 2

5.1 Introduction

As discussed in Chapter Four, a knowledge of the kinetics of reaustenitisation is vital in understanding and predicting the microstructure of heat affected zones in laser, electron beam and arc welds, and in many other applications where the steel undergoes a transient temperature rise into the $\alpha+\gamma$ phase field. In Chapter Four, isothermal reaustenitisation from the starting microstructures acicular ferrite plus austenite ($\alpha_a+\gamma$) and bainite plus austenite ($\alpha_b+\gamma$) was discussed. In this Chapter, the overall transformation kinetics of reaustenitisation beginning with bainite and with acicular ferrite will be examined and an attempt will be made to interpret the results theoretically. The continuous heating transformation behaviours of homogenised and heterogeneous weld metals are also investigated in order to understand the effect of segregation on the transformation and rationalise a quantitative model, which allows the kinetics of reaustenitisation to be predicted as a function of heating rate, alloy composition and other variables.

This work is connected with some projects on welding, and the alloy used are weld deposits WB, WC1 and WC2. The chemical compositions of the weld deposits are listed in Table II.1. Alloys preparation and other experimental details are the same as presented in Chapter Four.

5.2 Kinetics of Reaustenitisation and Time-Temperature-Transformation Curve

A thermodynamic model for reaustenitisation has been presented in Chapter Four, and most of the experimental results have been explained, but the detailed kinetics of reaustenitisation have not been addressed as yet. In this section, kinetics of reaustenitisation and TTT (Time-Temperature-Transformation) curves are studied in order to approach the prediction of the overall transformation of reaustenitisation.

The process of reaustenitisation using homogenised weld metal HWB, beginning with the microstructure of acicular ferrite and austenite ($\alpha_a+\gamma$), or the microstructure of bainite and austenite ($\alpha_b+\gamma$) has been studied. It has been found that at the final stage of isothermal reaustenitisation at a specific temperature the amount of the transformation is the same for a starting microstructure of acicular ferrite and bainite. However, the kinetics of the transformation are found to be significantly different. Fig. V.1 shows the dilatometry of isothermal reaustenitisation at the initial stage of 300 seconds. For a starting microstructure of acicular ferrite and austenite, specimens austenitised at 1200°C

for 30 minutes were isothermally transformed at 460°C for 30 minutes and then, without cooling below 460°C, rapidly up-quenched to a temperature for isothermal transformation (as shown in Fig. V.1A, B and C). For a starting microstructure of bainite and austenite, specimens austenitised at 950°C for 10 minutes were isothermally transformed at the same 460°C for 30 minutes and then rapidly up-quenched to a temperature for isothermal transformation (as shown in Fig. V.1 D, E and F). It is clear that for the starting microstructure of acicular ferrite and austenite the transformation rate is very slow at 680°C as compared with that of bainite and austenite. However, as the isothermal reaustenitisation temperature increases, the transformation rate increases, and the difference of transformation rate between the two cases becomes small. The time taken for the detectable reaustenitisation has been measured (Table V.1), and the TTT curves are shown in Figure V.2. Due to the driving force of transformation, as the reaustenitisation temperature increases, the time taken for the minimum detectable austenite growth decreases rapidly. The 5% transformation TTT curves have also been calculated by converting the volume fraction change to the relative length change of dilatometry. The calculations are expressed as the following equation.

When the volume fraction of austenite increases by 0.05 during isothermal transformation, the relative length change ($\Delta L/L$) of dilatometry can be written as:

$$\frac{\Delta L}{L} = \frac{1}{3}\left[\frac{(a_\gamma^F)^3 V_\gamma^F + 2(a_\alpha^F)^3 (1-V_\gamma^F) - (a_\gamma^I)^3 V_\gamma^I - 2(a_\alpha^I)^3 (1-V_\gamma^I)}{(a_\gamma^I)^3 V_\gamma^I + 2(a_\alpha^I)^3 (1-V_\gamma^I)}\right] \qquad \text{(V.1)}$$

where
- a_γ^F = lattice parameter of austenite at final stage of reaustenitisation.
- a_γ^I = lattice parameter of austenite at initial stage of reaustenitisation.
- V_γ^F = volume fraction of austenite at final stage of reaustenitisation.
- V_γ^I = volume fraction of austenite at initial stage of reaustenitisation.
- a_α^F = lattice parameter of ferrite at final stage of reaustenitisation.
- a_α^I = lattice parameter of ferrite at initial stage of reaustenitisation.

therefore $V_\gamma^F = 0.05 + V_\gamma^I$ (V.2)

If small change in the carbon concentration of the austenite is ignored, then:

$$a_\gamma^F \approx a_\gamma^I \tag{V.3}$$

$$\text{also} \quad a_\alpha^F \approx a_\alpha^I \tag{V.4}$$

Combining equation V.1,2,3 and 4, the relative length change ($\Delta L/L$) can be simply described as:

$$\frac{\Delta L}{L} = \frac{1}{3}\left[\frac{0.05\,(a_\gamma^I)^3 - 0.1\,(a_\alpha^I)^3}{(a_\gamma^I)^3 V_\gamma^I + 2(a_\alpha^I)^3(1-V_\gamma^I)}\right] \tag{V.5}$$

From the relative length change corresponding to an increase of 0.05 in volume fraction of austenite at specific isothermal reaustenitisation temperature, and dilatometric data, the transformation time has been obtained (Table V.2). The corresponding transformation TTT curves were plotted in Figure V.3. The results also show that as the reaustenitisation temperature increases, the time taken for increasing the volume fraction of austenite by 0.05 decreases rapidly in the case of $\alpha_a+\gamma$ or $\alpha_b+\gamma$.

5.2.1 Theory of the Kinetics of Reaustenitisation

A theory has been developed in order to predict the time taken for a detectable amount (or some specific amount) of reaustenitisation from bainite plus austenite (or acicular ferrite plus austenite). Because the nucleation of austenite is unnecessary when using high heating rates, reaustenitisation occurs only by the diffusional growth of austenite. Due to austenite layer thickening, the simplest treatment for growth of austenite from a mixture of bainitic ferrite and austenite is a one-dimensional growth model, involving the movement of a planar α/γ interface. This theory also assumes only carbon diffusion controlled growth* of austenite into ferrite, and a lack of soft impingement. It is presumed that for the early stages of transformation the austenite and ferrite are both semi-infinite in extent. The increase in half thickness of austenite can be described as [33].

$$q = \alpha_1 t^{1/2} \tag{V.6}$$

$$dq = 0.5\alpha_1 t^{-1/2} dt \tag{V.7}$$

* In fact, the microanalysis results (in Chapter Four) indicate diffusion also of substitutional elements. However, if local equilibrium is even approximately achieved at the transformation interface, then the carbon diffusion controlled growth rate calculated using the equilibrium carbon concentration would not differ from that for the diffusion of substitutional elements. Of course, the choice of the tie line governing the interface composition is then in principle complicated by the need to ensure main balance for all the elements at the interface. In general such a tie line will not pass through the average composition of the alloy, but here the assumption is made such that it does pass through the average carbon concentration. This may be a good approximation since the alloy is in this sense dilute.

where q is the increase in half thickness of austenite layer, starting thickness a_o, and α_1 is one dimensional parabolic thickening rate constant.

The schematic diagrams in Figure V.4 show the original austenite layer and the thickening austenite layer. c is the biggest side in three dimensions of bainitic ferrite plate, (it is usually supposed [25] that a ferrite plate is idealized as a rectangular parallelopiped with sides of length a, b and c, and c = b >> a), therefore c^2 is the boundary area of γ/α interface. The minimum detectable volume fraction change can be written as:

$$\Delta V_v = 2\, N_v c^2 \int_o^{\Delta a_m/2} dq \qquad (V.8)$$

where N_v is the initial number of particles of austenite per unit volume,
and Δa_m is the minimum detectable thickness increase (as shown in Figure V.4b).

Combining equations V.7 and 8, the minimum detectable volume fraction change can be expressed as:

$$\Delta V_V = 2\, N_v c^2 \int_0^{\tau} 0.5\alpha_1 t^{-1/2}\, dt \qquad (V.9)$$

where τ is the time taken for the minimum detectable transformation.

After integration,

$$\Delta V_v = 2\, \alpha_1 N_v c^2 \tau^{1/2} \qquad (V.10)$$

$$\text{hence} \quad \tau = \left(\frac{\Delta V_v}{2\alpha_1 N_v c^2}\right)^2 \qquad (V.11)$$

$$\text{however } 2N_v c^2 = S_v = \frac{2}{\bar{L}}$$

$$\text{therefore} \quad \tau = \left(\frac{\Delta V_v}{\alpha_1 S_v}\right)^2 \qquad (V.12)$$

where S_v is surface area of γ/α boundary per unit volume, and $(1/\bar{L})$ is the number of

intercepts of γ/α boundary per unit length of test line. From equation V.12 it is clear that the value of τ is dependent on not only parabolic rate constant (α_1) but also the surface area of γ/α interface per unit volume (S_v) for a specific amount of reaustenitisation. For the same starting microstructure and a specific amount of transformation τ decreases rapidly as the isothermal reaustenitisation temperature increases due to the α_1 increasing. This equation also indicates that the morphology of the starting microstructure will effect τ, because S_v is definitely governed by the starting microstructural morphology. Maybe this is the reason why $\alpha_b+\gamma$ and $\alpha_a+\gamma$ have different kinetic behaviours during reaustenitisation.

In the case of specific amount of reaustenitisation for the same starting microstructure, the equation V.12 can be simplified as the following relation:

$$\tau \propto \frac{1}{\alpha_1^2} \qquad \text{(V.13)}$$

5.2.2 Determination of Parabolic Thickening Rate Constant

α_1 value can be deduced by applying Fick's law of diffusion and the principle of conservation of mass. Figure V.5 shows the carbon concentration profiles in α and γ before reaustenitisation and during reaustenitisation. In Figure V.5a, the carbon concentration of γ is the same C_1 before reaustenitisation. In Figure V.5b, the carbon concentration of γ at γ/α interface during reaustenitisation is $C^{\gamma\alpha}$, and the carbon concentration of γ far away from the interface remains C_1. It is assumed that the carbon concentration of α remains the same, $C^{\alpha\gamma}$, before and during reaustenitisation. Co-ordinate Z is defined normal to γ/α interface.

During reaustenitisation the flux of carbon toward γ/α interface, at the position of interface can be expressed as:

$$J = -D_{11}\{C^{\gamma\alpha)}\}\ \frac{\partial C}{\partial Z} \qquad \text{(V.14)}$$

The diffusion coefficient of carbon in austenite, D_{11}, is known to be strongly concentration dependent [168]. The weighted average diffusivity, $\bar{D}_{11}$, can adequately represent the effective diffusivity of carbon [169], and is given by:

$$\bar{D}_{11} = \int_{C_1}^{C^{\alpha\gamma}} D_{11}\, dC/(C^{\alpha\gamma} - C_1) \qquad \text{(V.15)}$$

The rate at which carbon concentration of γ is diluted can be written as:

$$R = \upsilon (C_1 - C^{\alpha\gamma}) \tag{V.16}$$

where υ is the velocity of interface.

Because the position of interface along co-ordinate z can be described as:

$$Z = \alpha_1 t^{1/2}$$

$$\text{therefore} \quad \upsilon = \frac{dZ}{dt} = \frac{1}{2}\alpha_1 t^{-1/2} \tag{V.17}$$

Combining equation V.16 and 17, the rate at which carbon concentration of γ is diluted can be expressed as:

$$R = (C_1 - C^{\alpha\gamma})(\alpha_1 t^{-1/2})/2 \tag{V.18}$$

Conservation of mass at the interface requires that (i.e., combining equations V.14 and 18):

$$(C_1 - C^{\alpha\gamma})(\alpha_1 t^{-1/2})/2 = -\bar{D}_{11}\{C^{\gamma\alpha}\}(\partial C/\partial Z)_{z=Z} \tag{V.19}$$

where z is the co-ordinate normal to the interface plane and Z is the position of the interface along co-ordinate z. Equation V.19 simply states that the amount of carbon partitioned from the γ, per unit time equals the carbon flux away from the γ/α interface. From Fick's laws, the differential equation for the matrix is given by:

$$\partial C/\partial t = \partial(\bar{D}_{11}\{C\}(\partial C/\partial Z))/\partial Z \tag{V.20}$$

subject to the boundary condition $C = C^{\gamma\alpha}$ at $z = Z\{t\}$, and $C = C_1$ at $t = 0$, and equation V.19.

The equation has been solved [25] to give an implicit relation for α_1 as a solution of the form:

$$f_1 = H_1\{\bar{D}_{11}\} = \frac{C_1 - C^{\gamma\alpha}}{C_1 - C^{\alpha\gamma}} \tag{V.21}$$

where

$$H_1\{\bar{D}_{11}\} = (0.25\pi/\bar{D}_{11})^{0.5}\ \alpha_1[\mathrm{erfc}\{0.5\alpha_1/(\bar{D}_{11})^{0.5}\}]\exp\{\alpha_1^2/(4\bar{D}_{11})\} \qquad (V.22)$$

Finally the α_1 can be calculated from equation V.21 and 22.

5.2.3 The Relation between the Parabolic Rate Constant and TTT Curves

The parabolic thickening rate constant (α_1) at different reaustenitisation temperatures has been calculated using the computer program and the data given in Table V.3. An attempt was then made to find the relation between the time taken (τ) for the detectable amount (or some specific amount) of reaustenitisation from starting microstructures bainite plus austenite ($\alpha_b+\gamma$) and acicular ferrite plus austenite ($\alpha_a+\gamma$). Figure V.6 and 7 show τ is experimentally found to be proportional to $1/\alpha_1^2$. In Figure V.6 for detectable amount of transformation, the correlation coefficients for the linear relation between τ and $1/\alpha_1^2$ were found to be 0.99 and 0.97, in the case of starting microstructure $\alpha_a+\gamma$ and $\alpha_b+\gamma$ respectively. In the case of volume fraction of γ increasing by 0.05, Figure V.7 presents correlation coefficients for above linear relation to be 0.91 and 0.96 for starting microstructure $\alpha_a+\gamma$ and $\alpha_b+\gamma$, respectively. In Figure V.2 and 3, it is shown that at the same reaustenitisation temperature, the time taken (τ) for detectable amount (or 0.05) transformation is longer with the starting microstructure $\alpha_a+\gamma$ than with the starting microstructure $\alpha_b+\gamma$. For these two different starting microstructures, the mean number of intercepts $(1/\bar{L})$of γ/α boundary per unit length of test line in each case has been measured on transmission electron micrographs (using 50 test lines at random on 5 electron micrographs magnified by 10000X for the two different starting microstructures, respectively). The results are $(1/\bar{L})$= 0.78 ± 0.15 μm^{-1} for $\alpha_a+\gamma$, and $(1/\bar{L})$= 1.07 ± 0.12μm^{-1} for $\alpha_b+\gamma$. Therefore the surface area can be determined as well; S_v = 1.56±0.30μm^{-1} for $\alpha_a+\gamma$ and S_v = 2.14±0.24μm^{-1} for $\alpha_b+\gamma$.

For a specific amount of reaustenitisation, the equation V.12 can be expressed as:

$$\tau \propto 1/(S_v\alpha_1)^2 \qquad (V.23)$$

It is clear that the amount of γ/α grain boundary area per unit volume is an important factor. That is the reason why the value of τ is larger in the case of $\alpha_a+\gamma$. The transformation kinetics of reaustenitisation from $\alpha_a+\gamma$, or $\alpha_b+\gamma$ can then be understood.

5.3 Continuous Heating Transformation

High speed dilatometry was used to study the continuous heating transformation of unhomogenised and homogenised weld metals. The as-deposited weld metals used were

WB, WC1 and WC2, and the corresponding homogenised weld metals were designated as HWB, HWC1 and HWC2. The dilatometer specimens were heated from room temperature to 950°C at different heating rates of 0.06 - 56 °C/s. Figures V.8,9 and 10 show the relative length change and temperature profiles, monitored by the chart recorder on the dilatometer during continuous heating. From the profiles, the transformation start temperature has been obtained, and the curves for transformation start temperature versus heating rate are plotted in Figure V.11 and 12.

For all homogenised and unhomogenised weld metals, there was no decomposition during heating even at a very slow heating rate, 0.06 °C/s, as shown in Figure V.8,9 and 10. From the experimental continuous heating transformation curves in Figure V.11, it is evident that homogenised weld metals transform at higher temperature than unhomogenised weld metals in all cases. This is to be expected due to the segregation in unhomogenised weld metals. Alloying elements are not uniformly distributed in as-deposited weld metals, and solute-rich areas will transform to austenite earlier than regions containing average levels of alloying elements. However, at the same heating rate the difference of transformation start temperature between homogenised weld metals and unhomogenised weld metals is only about 10°C. This is presumably because the degree of segregation is not so large. It has been shown [70] that in carbon containing 0.68 wt% steel weld deposit, columnar austenite grain consists of a bundle of fine regular hexagonal cell all having approximately the same crystallographic orientation in space. For the weld metals studied in this investigation, the segregation cell structure within the columnar austenite grain has not been found as yet. This is probably because the segregation is not heavy, therefore this kind of cell structure is difficult to reveal.

In Figure V.12, the continuous heating transformation behaviours among the homogenised weld metals HWB, HWC1 and HWC2, and among the unhomogenised weld metals WB, WC1 and WC2 can be compared. In Figure V.12(a), it has been shown that continuous transformation curves of HWC1 and HWC2 are nearly at the same position, but that of HWB is about 15°C below. similar results were presented for unhomogenised weld metals WC1, WC2 and WB (Figure V.12(b). The M_S temperatures for homogenised weld metals studied have been calculated as shown in Figure II.1(a), and are 400, 425 and 427°C for HWB, HWC1 and HWC2, respectively. The M_S temperature of HWB is significantly lower than that of the other two weld metals. The carbon concentration of residual austenite can be calculated from the T'_0 curve at M_S temperature, although at ambient temperature some austenite will transform to martensite. The carbon content of retained austenite will effect the reaustenitisation process, and this is the reason why the transformation start temperature for HWB (or WB) is lower.

5.4 Conclusions

A theory of kinetic isothermal reaustenitisation for starting microstructures $\alpha_a+\gamma$ and $\alpha_b+\gamma$ has been proposed, and it has very good agreement with experimental data. This theory indicates that for a specific amount of reaustenitisation, the transformation time is governed by not only parabolic rate constant (α_1) but also the surface area of γ/α boundary per unit volume. In the same volume fraction of α_a and α_b for starting microstructures of $\alpha_a+\gamma$ and $\alpha_b+\gamma$, the reaustenitisation rate at specific temperature for $\alpha_b+\gamma$ is faster than for $\alpha_a+\gamma$, simply because the surface area of γ/α boundary per unit volume for $\alpha_b+\gamma$ is larger. Using this theory the Time-Temperature-Transformation curve of isothermal reaustenitisation can be predicted.

The continuous heating transformation for homogenised and unhomogenised weld metals has been studied using dilatometry at a wide range of heating rates. It is found that at the same heating rate the difference of transformation start temperature between homogenised and unhomogenised weld metals studied is not so significant, and it is assumed that the degree of segregation in weld metals studied is not very large. In this study the carbon concentration of austenite has also strong influence on the reaustenitisation although the starting microstructure may consist of more than three phases - acicular ferrite (bainite), martensite and austenite etc.

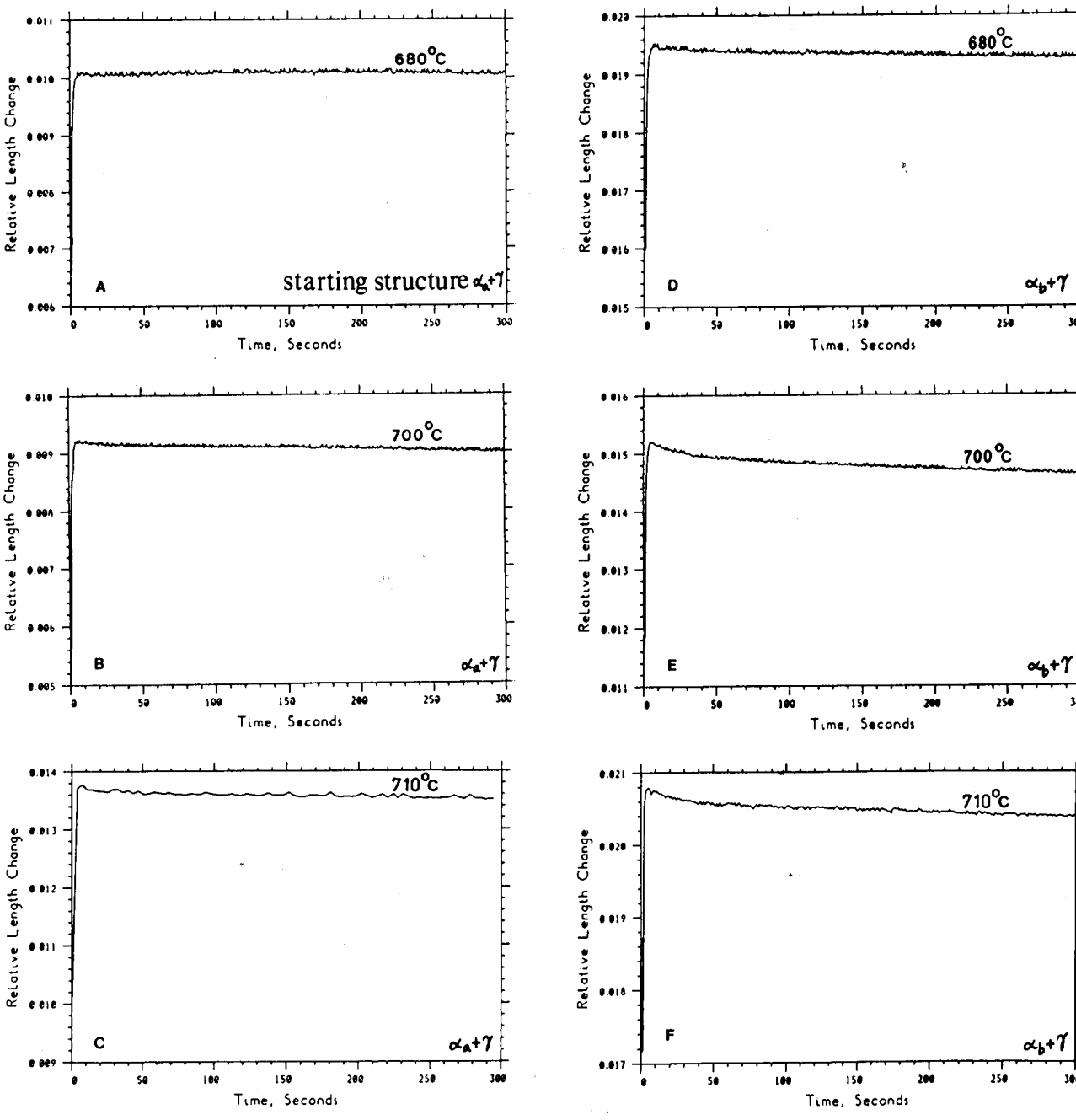

Figure V.1 - Showing the dilatometry of isothermal reaustenitisation at the initial stage of 300 seconds. (A),(B) and (C) for starting microstructure of $\alpha_a+\gamma$; (D), (E), and (F) for starting microstructure of $\alpha_b+\gamma$.

Table V.1 - The Time Taken for the Detectable Reaustenitisation in the Case of Starting Microstructure $\alpha_a+\gamma$ and $\alpha_b\gamma$.

Temperature (°C)	$\alpha_a+\gamma$ Time (Seconds)	$\alpha_b+\gamma$ Time (Seconds)
680	250	30
690	90	15
700	30	6
710	10	4
720	5	3

Table V.2 - The Time Taken for Increasing the Volume Fraction of γ by 0.05 in the Case of Starting Microstructures $\alpha_a+\gamma$ and $\alpha_b+\gamma$.

Temperature (°C)	$\alpha_a+\gamma$ Time (Seconds)	$\alpha_b+\gamma$ Time (Seconds)
680	548	300
690	370	150
700	192	110
710	114	70
720	43	26

Table V.3 - The Parabolic Constant (α_1) at Different Reaustenitisation Temperature.

Temperature (°C)	α_1(cm/s$^{0.5}$)	$1/\alpha_1^2$ (s/cm^2)
680	0.9968×10^{-5}	0.1006×10^{11}
690	0.2017×10^{-4}	0.2459×10^{10}
700	0.3350×10^{-4}	0.8911×10^{9}
710	0.5679×10^{-4}	0.3101×10^{9}
720	0.8300×10^{-4}	0.1452×10^{9}

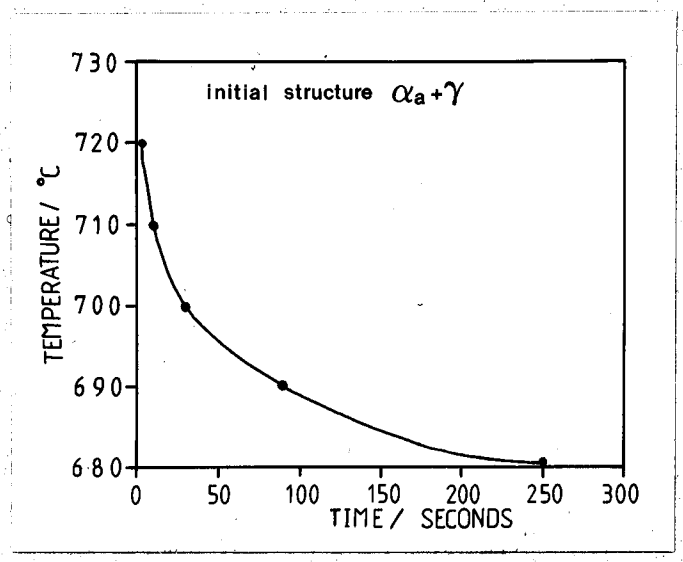

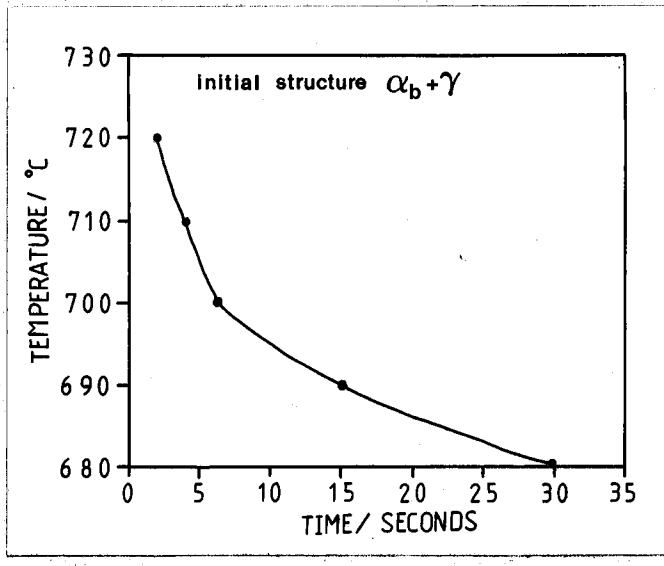

Figure V.2 - TTT curves of reaustenitisation of minimum detectable austenite growth. (a) starting microstructure $\alpha_a+\gamma$; (b) starting microstructure $\alpha_b+\gamma$.

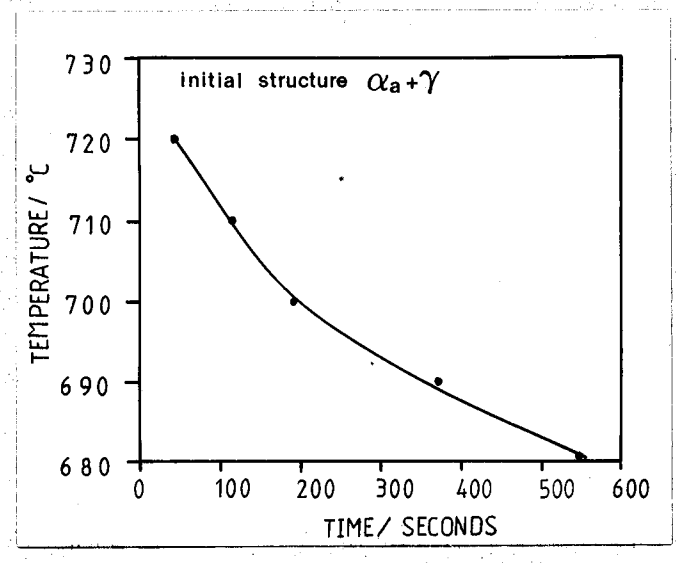

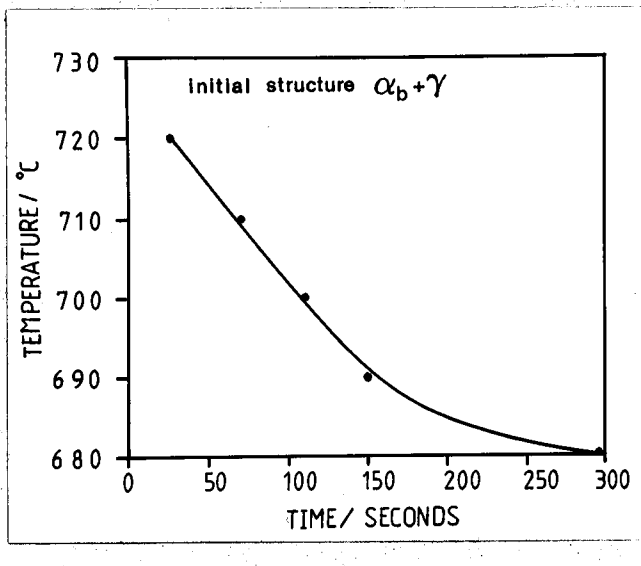

Figure V.3 - TTT curves of reaustenitisation for increasing austenite volume fraction by 0.05. (a) starting microstructure $\alpha_a+\gamma$; (b) starting microstructure $\alpha_b+\gamma$.

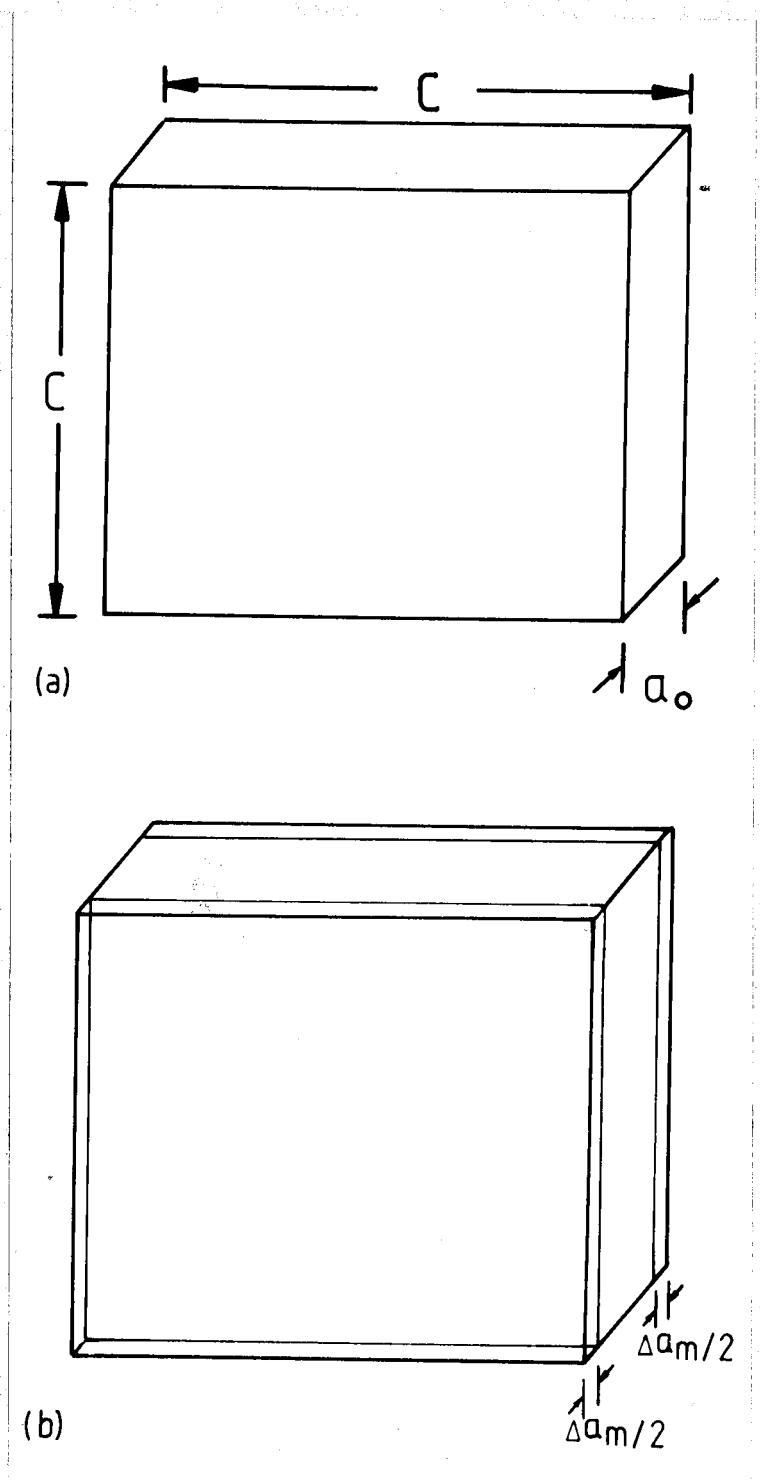

Figure V.4 - Schematic diagrams showing (a) the original layer of austenite before reaustenitisation and (b) the thickening layer of austenite during reaustenitisation.

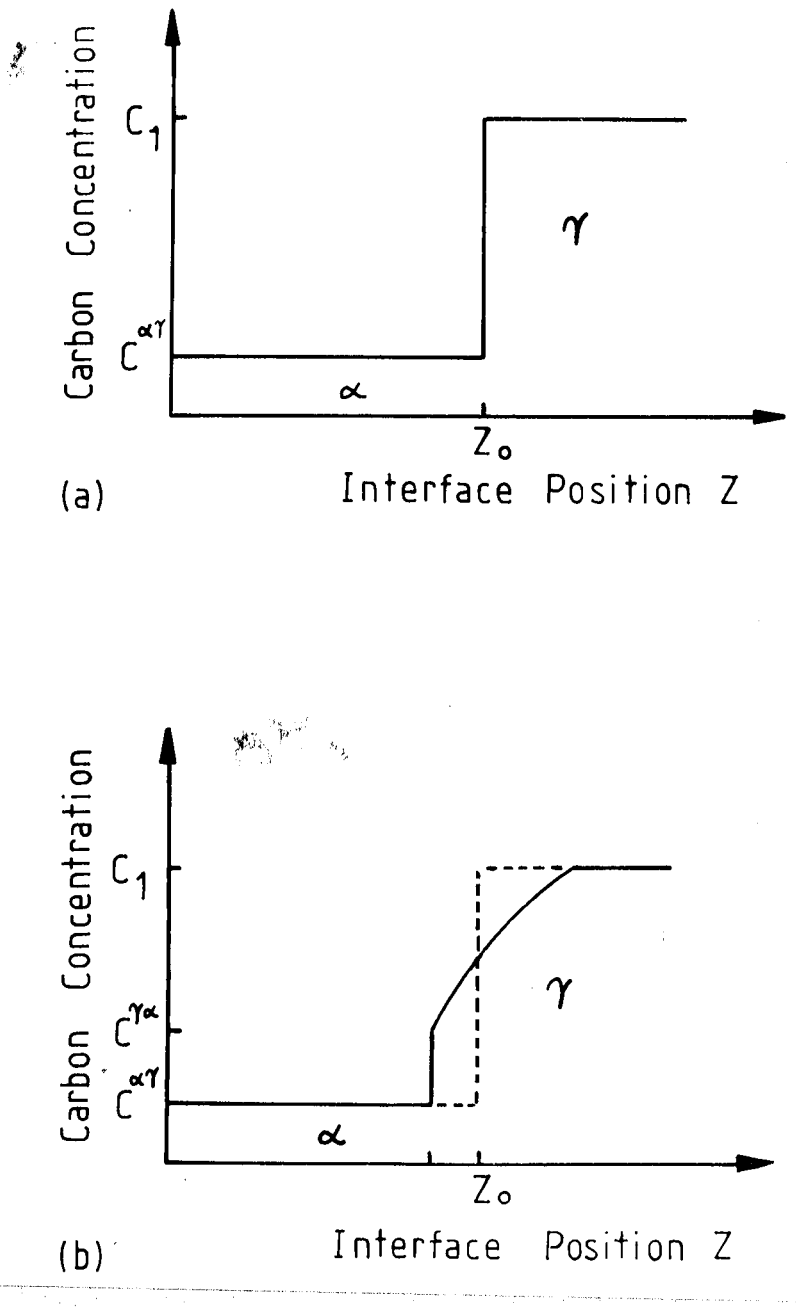

Figure V.5 - Showing the carbon concentration profile (a) before reaustenitisation and (b) during reaustenitisation. The interface position (Z) is defined normal to the γ/α interface. C_1 is carbon concentration in γ, $C^{\gamma\alpha}$ is carbon concentration in γ at γ/α interface during reaustenitisation, and $C^{\alpha\gamma}$ is carbon concentration in α at α/γ interface during reaustenitisation.

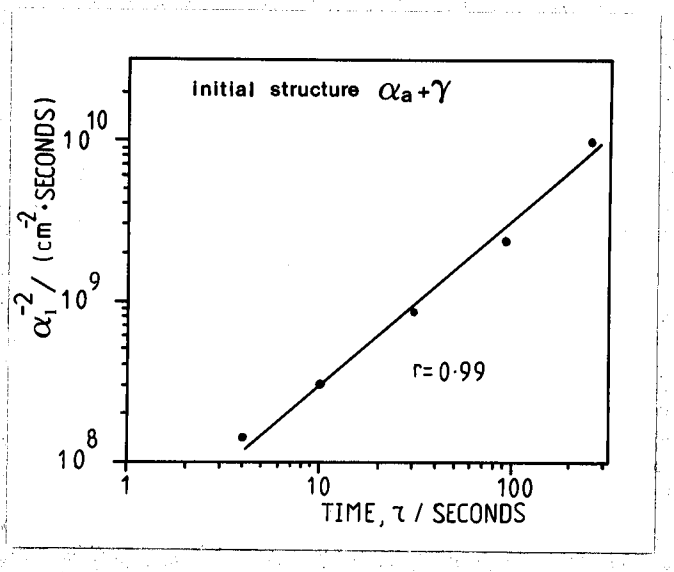

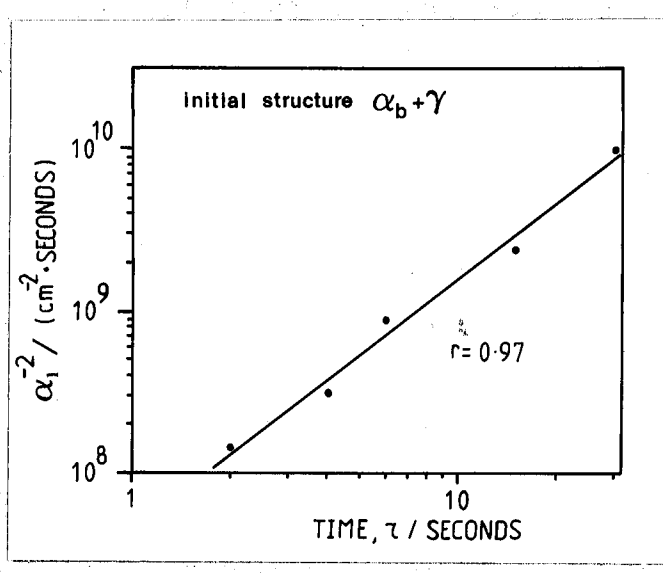

Figure V.6 - Showing that the time taken for detectable amount of transformation (τ) is proportional to $1/\alpha_1^2$. (a) In the case of initial structure $\alpha_a+\gamma$, the correlation coefficient for the above linear relation was found to be 0.99; and (b) in the case of initial structure $\alpha_b+\gamma$, the correlation coefficient to be 0.97.

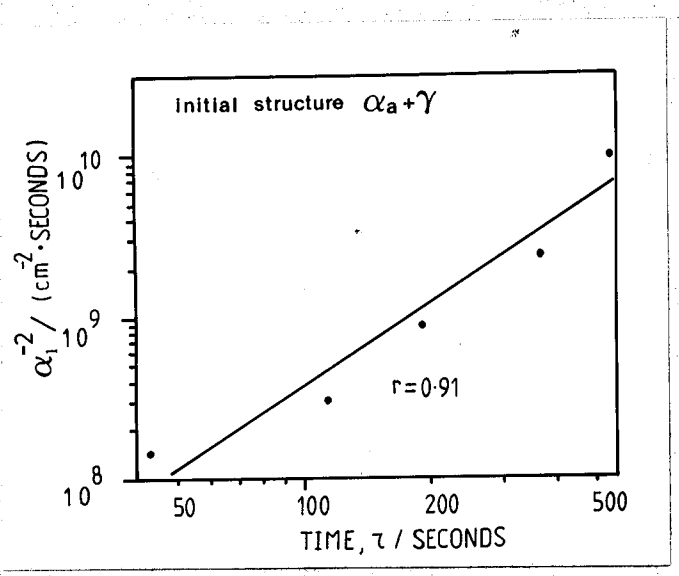

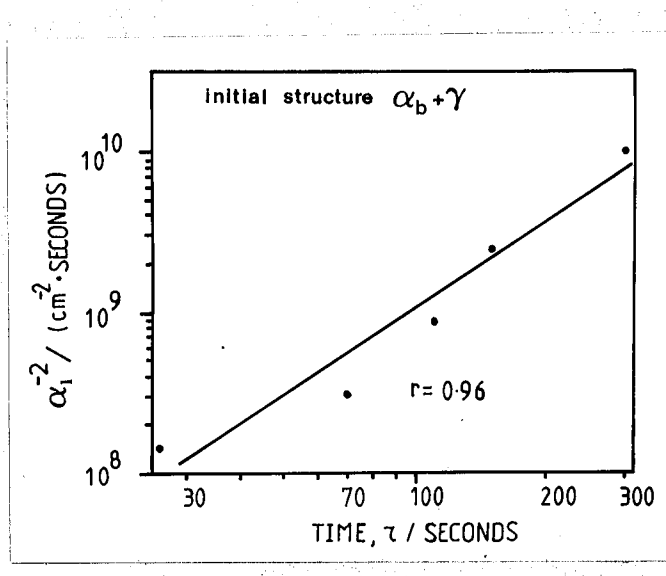

Figure V.7 - Showing that the time taken for increasing volume fraction of γ by 0.05, τ, is proportional to $1/\alpha_1^2$. (a) In the case starting microstructure $\alpha_a+\gamma$, the correlation coefficient for the above linear relation was found to be 0.91; and (b) in the case of starting microstructure $\alpha_b+\gamma$, the correlation coefficient to be 0.96.

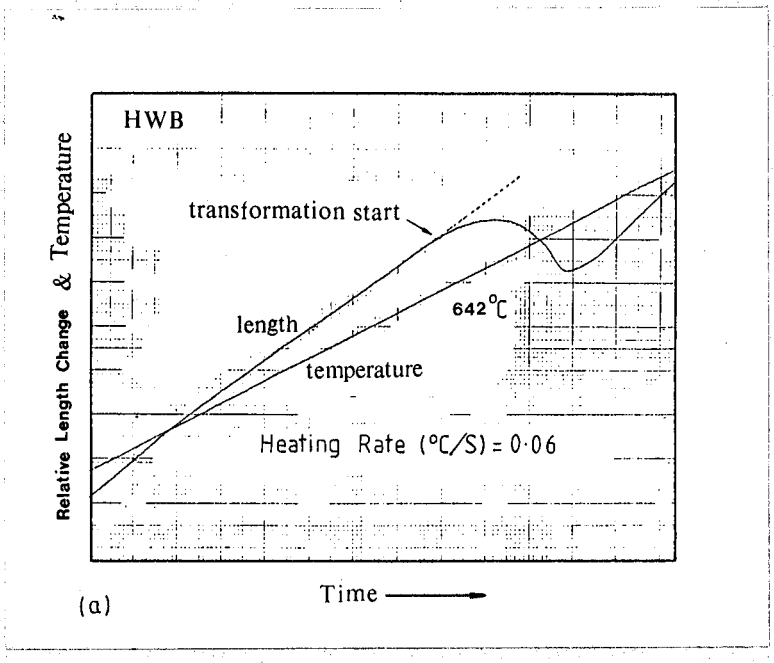

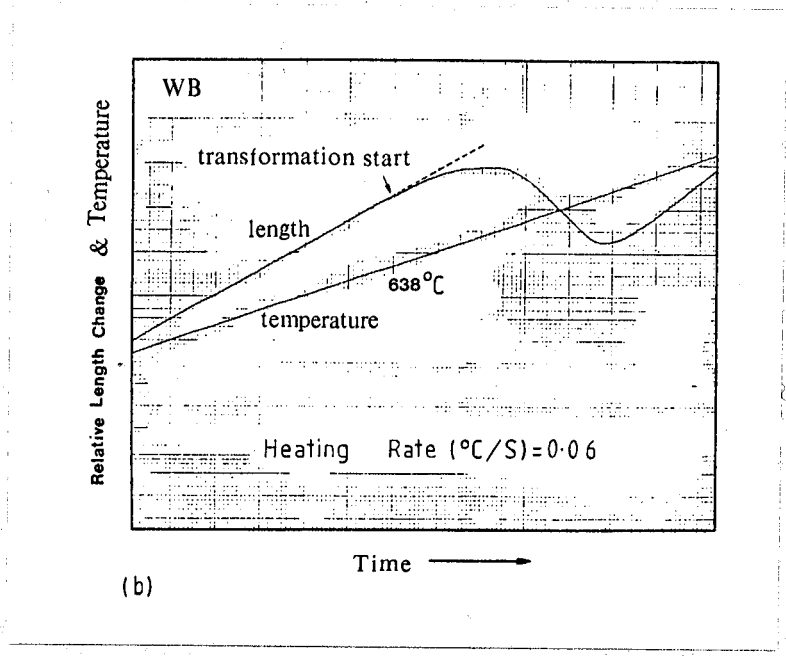

Figure V.8 - Showing the relative length change and temperature profiles on dilatometry during continuous heating for weld metals HWB and WB, monitored by the chart recorder.

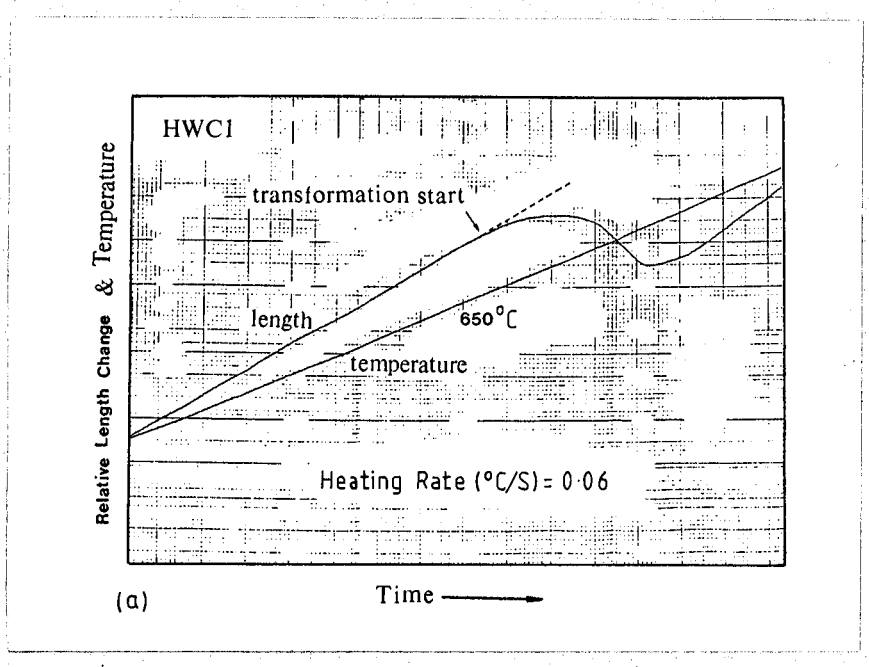

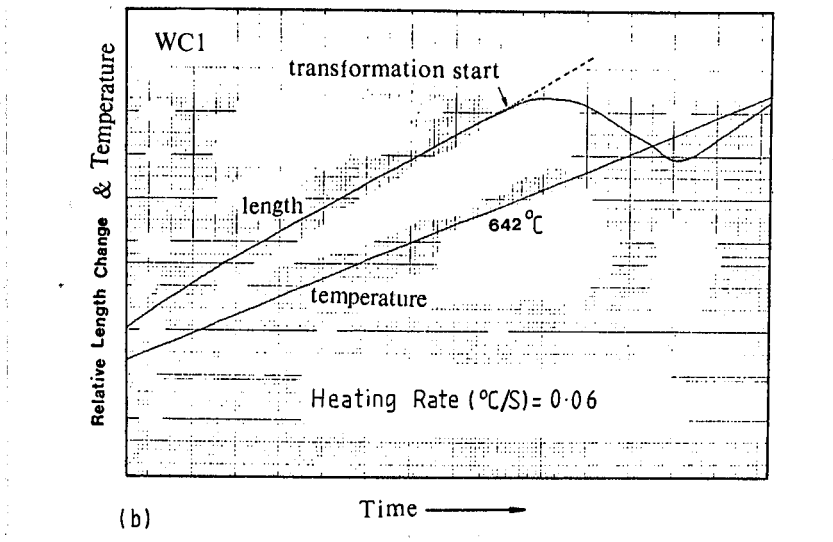

Figure V.9 - Showing the relative length change and temperature profiles on dilatometry during continuous heating for weld metals HWC1 and WC1, monitored by the chart recorder.

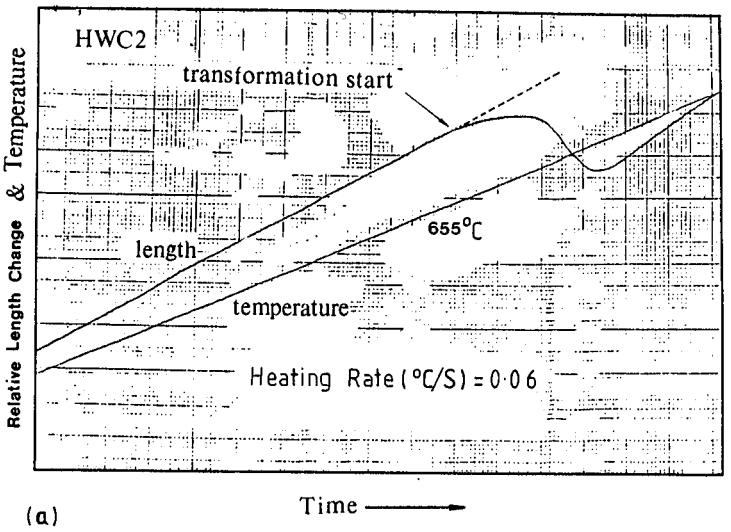

(a)

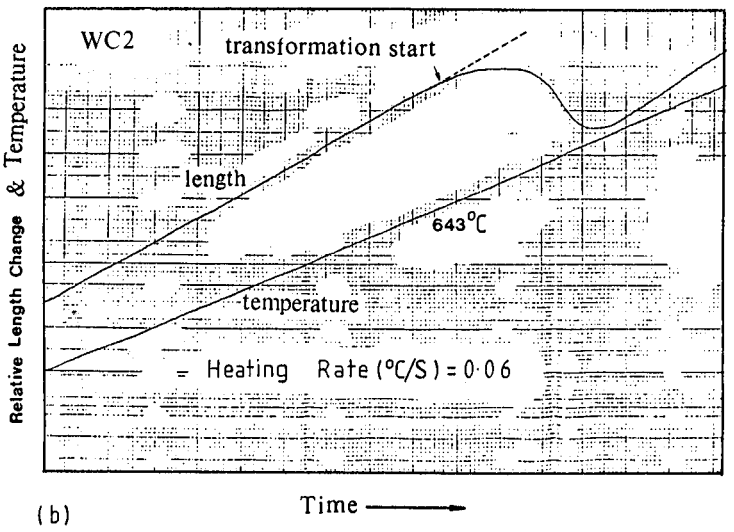

(b)

Figure V.10 - Showing the relative length change and temperature profile on dilatometry during continuous heating for the weld metals HWC2 and WC2, monitored by the chart recorder.

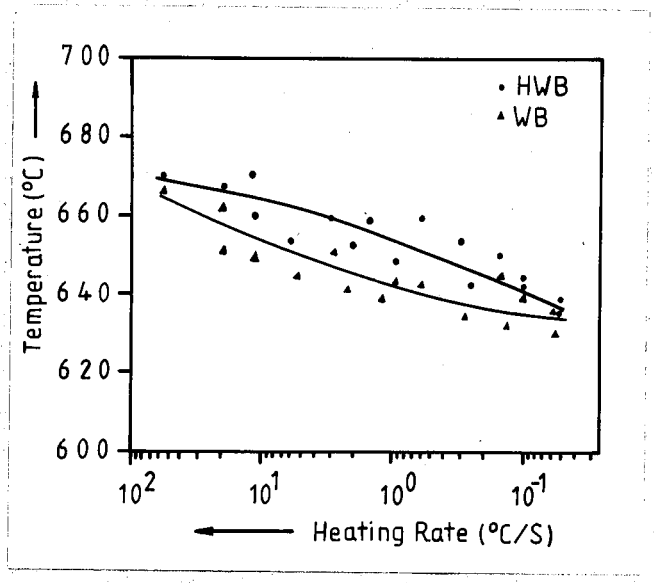

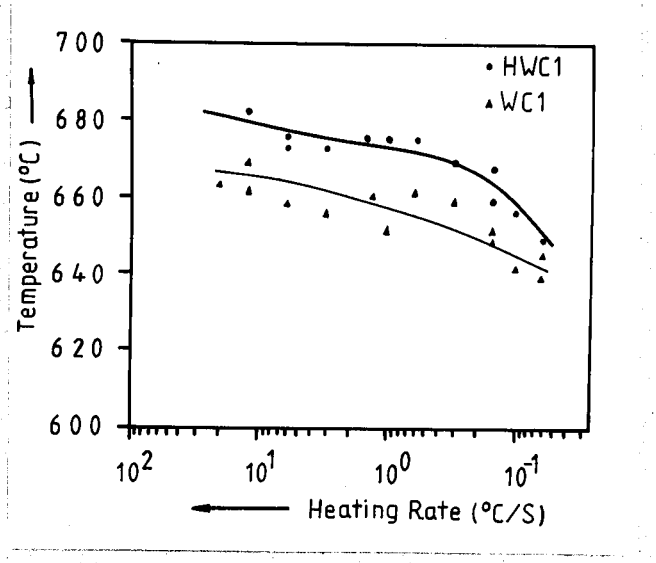

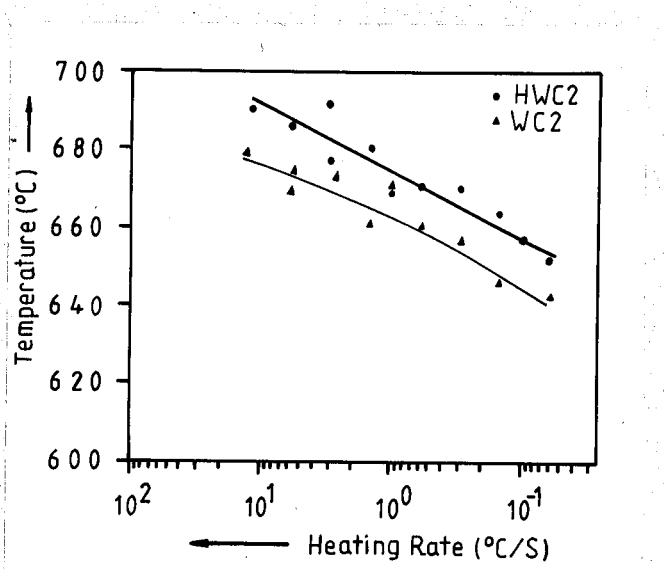

Figure V.11(a)(b)(c) - Showing continuous heating transformation curves (transformation start temperature versus heating rate) for HWB, WB, HWC1, WC1, HWC2 and WC2.

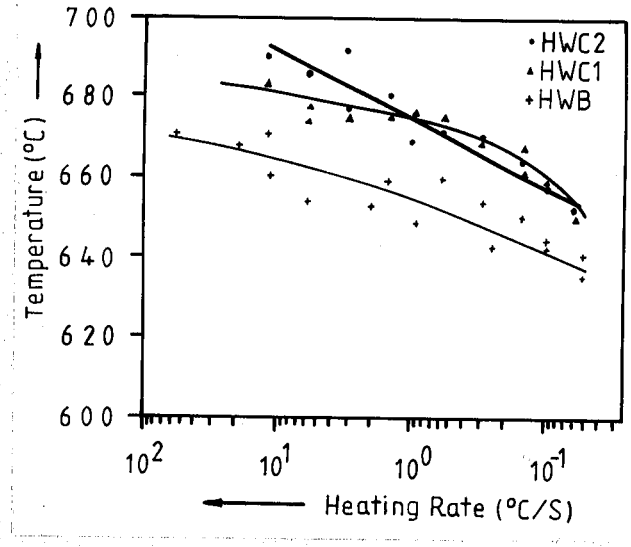

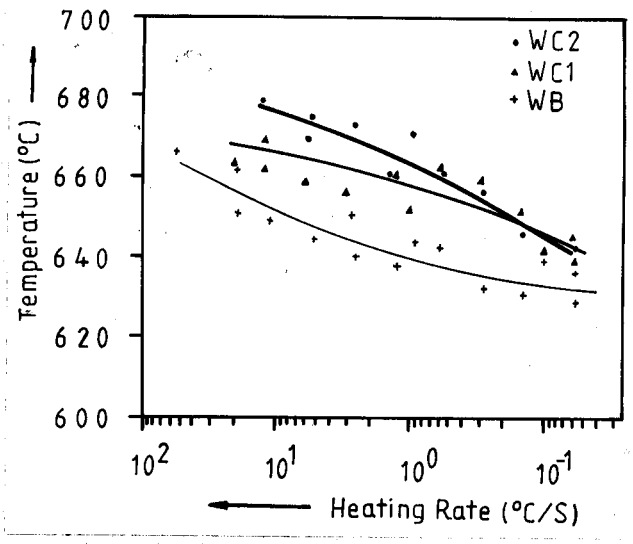

Figure V.12 - Showing continuous heating transformation curves (transformation start temperature versus heating rate) for (a) homogenised weld metals HWB, HWC1 and HWC2, (b) as-deposited weld metals WB, WC1. and WC2.